iodosomethane, while the remainder may rearrange or dissociate. No evidence was found for further reaction of the O_2 byproduct.

During the second period of irradiation, this time at 290–420 nm, the iodomethane–ozone molecular complex is already depleted and iodosomethane is photodecomposed. Since neither uncomplexed ozone nor iodomethane is affected by this radiation, iodosomethane must be a common precursor to all the photoproducts. Excited iodosomethane may eliminate HI directly or rearrange to methyl iodate or iodomethanol, which can eliminate HI (Scheme II). While these experiments do not provide incontrovertible evidence for the detection of methyl hypoiodite and iodomethanol compounds in the photodecomposition of iodosomethane, several absorptions have been observed in the relevant "fingerprint" regions of their infrared spectra. Either could also be a suitable precursor to formaldehyde and hydrogen iodide, and with regard to the formation of two complexed formaldehyde species on photolysis, it may be significant that methyl hypoiodite would give a formaldehyde–hydrogen iodide molecular pair in the wrong orientation for hydrogen bonding to occur. When the matrix is warmed, rotation of HI could occur, and as the formaldehyde and hydrogen iodide are formed in such close proximity, it is hardly surprising that all of the less stable formaldehyde complex is depleted. While the occurrence of two different HI and formaldehyde complexes after photolysis is not, of course, proof that methyl hypoiodite and iodomethanol are acting as precursors to differently oriented molecular pairs (either precursor could produce excited hydrogen iodide with enough energy to rotate into or away from the correct orientation for hydrogen bonding to occur), the possibility exists. Work on chemical laser[20] systems provides supporting evidence that iodomethanol might be expected to yield formaldehyde; Lin proposed the reaction of ^1D oxygen atoms with chloromethanes $Cl_{4-n}CH_n$ to give chloromethanols, $Cl_{4-n}CH_{n-1}OH$ (n = 1–3), which serve as precursors for hydrogen chloride and chlorinated formaldehyde $H_xCl_{2-x}CO$ (x = 0–2). Furthermore, elimination of hydrogen iodide from iodomethanol places the acid hydrogen adjacent to the carbonyl oxygen and facilitates formation of the hydrogen-bonded complex **5**. Finally, the above photochemical pathway has distinct analogies to that reported for CH_3NO_2 and CH_3ONO, which photolyze to give the H_2CO--HNO complex.[21,22]

The small yield of CH_3IO_2 can be accounted for by a similar mechanism to that proposed for formation of $ClIO_2$,[5] which involves further reaction between iodosomethane and oxygen atoms released by decomposition of excited iodosomethane.

Conclusions

Codeposition of iodomethane and ozone in argon matrices leads to the formation of a molecular complex between iodomethane and ozone, which exhibited a 395-nm absorption band and photodissociated with 360–470-nm mercury-arc radiation presumably involving a charge-transfer mechanism. The iodosomethane photoproduct, CH_3IO, is probably formed initially with excess internal energy; this excited intermediate species is either quenched by the matrix or it rearranges to iodomethanol (ICH_2OH) or methyl hypoiodite (CH_3OI) or it eliminates HI. The infrared spectrum of iodosomethane is closely related to that of the parent iodomethane, and the I–O bond is weaker than that found in iodosyl chloride.

Photodecomposition of the quenched iodosomethane can be initiated by irradiation at 290–420 nm. The yields of both iodomethanol and methyl hypoiodite are thereby increased as are those of two formaldehyde–hydrogen iodide molecular complexes. Both iodomethanol and methyl hypoiodite can also serve as precursors to the photoproducts involving formaldehyde, the latter formed by elimination of hydrogen iodide from the precursors. Warming the matrix leads to a reduction in several photoproducts; however, the formaldehyde–HI hydrogen-bonded complex increased at the expense of the other formaldehyde–HI complex. Indeed depletion of the latter is complete under these conditions and is a consequence of the proximity of the hydrogen iodide molecule on photodecomposition of the precursors. The infrared spectrum of the complex can be measured without interference from that of either parent and is consistent with a hydrogen-bonded structure.

Acknowledgment. The authors gratefully acknowledge the donors of the Petroleum Research Fund, administered by the American Chemical Society, for support of this research and S. R. Davis for preparing the figures.

Registry No. CH_3I, 74-88-4; O_3, 10028-15-6; $^{18}O_3$, 21424-26-0; CD_3I, 865-50-9; CH_3IO, 97551-34-3; ICH_2OH, 50398-30-6; CH_3OI, 26466-04-6; HI, 10034-85-2; CH_2O, 50-00-0; Ar, 7440-37-1.

(20) Lin, M. C. *J. Phys. Chem.* **1972**, *76*, 811.
(21) Jacox, M. E.; Rook, F. L. *J. Phys. Chem.*, **1982**, *86*, 2899.
(22) Müller, R. P.; Huber, J. R. *J. Phys. Chem.* **1983**, *87*, 2460.

Contribution from the Department of Chemistry and Institute of Colloid and Surface Science, Clarkson University, Potsdam, New York 13676

Thermodynamics and Kinetics of Aqueous Ferric Phosphate Complex Formation†

RICHARD B. WILHELMY,‡ RAMESH C. PATEL,* and EGON MATIJEVIĆ*

Received September 15, 1983

The equilibria and kinetics of complexation of iron(III) with phosphoric acid (at pH <2) were studied at 25 and 50 °C at ionic strength μ = 2.5 M by using spectrophotometric and stopped-flow techniques. The results are consistent with the formation of two complexes, $FeH_2PO_4^{2+}$ and $Fe(H_2PO_4)_2^+$. The second species could only be detected by the analysis of kinetic data. The equilibrium constants, extinction coefficients, rate constants, and activation parameters for the formation of these complexes are given. A mechanism is proposed to account for the observed hydrogen ion dependency of the apparent forward rate constants.

Introduction

Complexation reactions between iron(III) and phosphate ions play an important role in soil chemistry, water treatment, and corrosion. Numerous investigators[1-22] have postulated the formation of various species (Table I), depending on the experimental conditions, methods of analysis, and interpretation of the results. Few studies, however, reported thermodynamic data (especially at elevated temperatures), and no kinetic information on these

†Supported by the American Iron and Steel Institute, Project No. 63-269, and the Electric Power Research Institute, Contract RP-966-2.
‡Part of a Ph.D. thesis. Presently at Alcoa Technical Center, Alcoa Center, PA 15069.

(1) Lanford, O.; Kiehl, E. *J. Am. Chem. Soc.* **1941**, *64*, 291.
(2) Banerjee, S. *J. Indian Chem. Soc.* **1950**, *27*, 417.
(3) D'Amore, G. *Atti Soc. Peloritana Sci. Fis., Mat. Nat.* **1956**, *3*, 95.
(4) Pilipenko, A. T.; Ivashchenko, L. N. *J. Gen. Chem. USSR* (*Engl. Transl.*) **1956**, *26*, 751.
(5) Galal-Gorchev, H.; Stumm, W. *J. Inorg. Nucl. Chem.* **1963**, *25*, 567.
(6) Lahiri, S. C. *J. Indian Chem. Soc.* **1965**, *42*, 715.
(7) Filatova, L. N.; Chepelevetskii, M. L. *Proc. Acad. Sci. USSR* **1966**, *166*, 49; *Russ. J. Inorg. Chem.* (*Engl. Transl.*) **1966**, *11*, 888.
(8) Bohn, H. L.; Peech, M. *Soil Sci. Soc. Am. Proc.* **1969**, *33*, 873.

0020-1669/85/1324-3290$01.50/0

Table I. Proposed Ferric Phosphate Complexes

complex	ref	complex	ref
$FeHPO_4^+$	1–3, 5, 6, 13, 15, 19, 21	$Fe(PO_4)_3^{6-}$	12, 15
		$Fe_2PO_4^{3+}$	4, 15, 21
$FeH_2PO_4^{2+}$	5, 8, 10, 18, 20	$Fe_2HPO_4^{4+}$	7, 11
$Fe(HPO_4)_2^-$	2, 17, 19	$Fe_2(OH)PO_4^{2+}$	11, 15, 16, 21
$Fe(H_2PO_4)_4^-$	22	$Fe_2(OH)HPO_4^{3+}$	21
$Fe(OH)PO_4^-$	9	$Fe_2H_3(PO_4)_2^{3+}$	20
$Fe(HPO_4)_3^{3-}$	12, 14, 21	$Fe_3H_6(PO_4)_4^{3+}$	20
$Fe(PO_4)_2^{3-}$	9		

species could be found. Recently, ferric phosphate hydrosols of narrow size distribution were generated by aging solutions containing ferric and phosphate ions at 40–50 °C.[23] In order to clarify which complexes play a role in the formation of the solid phase, UV/visible and stopped-flow spectroscopies were employed to identify the species and to determine the relevant thermodynamic and kinetic constants. This paper presents the results of this investigation under experimental conditions similar to those leading to hydrosol formation.

Experimental Section

Materials. Ferric perchlorate stock solutions were prepared by dissolving the anhydrous salt (G. F. Smith; anhydrous, nonyellow reagent) in doubly distilled water and by passing the resulting solution through 0.20-μm pore size Nuclepore membranes before use. These stock solutions were found to be stable over extended periods of time either in concentrations greater than 1 M or in the presence of a tenfold excess of perchloric acid. The solutions were analyzed spectrophotometrically as the iron-α,α'-dipyridyl complex.[24]

Perchloric acid (G. F. Smith; doubly distilled) and phosphoric acid (Baker) were used as supplied. The acid content of the stock solutions was determined by pH titrations with high-purity carbonate-free NaOH. Phosphate ion concentration was analyzed colorimetrically as an antimonyl phosphomolybdenum blue complex.[25] Solutions of sodium perchlorate (G. F. Smith; anhydrous reagent) were prepared with doubly distilled water and filtered by using a 0.20-μm pore size membrane.

Sample Preparation. The components were added in the following order: ferric perchlorate or phosphoric acid solution, $HClO_4$, $NaClO_4$, and water. The mixture was allowed to equilibrate overnight at room temperature prior to any measurements. Solutions used in the spectroscopic study were mixed in the stopped-flow apparatus. The ranges of concentrations investigated were 8.0×10^{-5} to 8.0×10^{-4} M in $Fe(ClO_4)_3$, 0 to 2.8×10^{-2} M in H_3PO_4, and 0.030 to 0.20 M in $HClO_4$. The concentration of $NaClO_4$ was maintained at 2.5 M in order to assure a constant ionic strength.

Spectrophotometric Measurements. All measurements were made on a Perkin-Elmer Model 553A UV/visible double-beam recording spectrophotometer. The temperature of the cell holder was controlled to ±0.1 °C by a Haake Model FS circulating water bath. Data were taken at 25 and 50 °C. The samples, contained in matched 1.0-cm or 1.0-mm stoppered quartz cells, were allowed to equilibrate for at least 15 min in the spectrophotometer before recording absorbances.

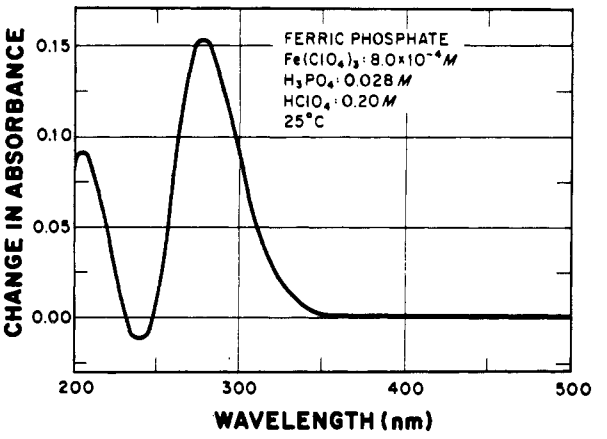

Figure 1. Change in absorbance as a function of the wavelength of a solution 8.0×10^{-5} M in $Fe(ClO_4)_3$, 2.9×10^{-2} M in H_3PO_4, 0.20 M in $HClO_4$, and 2.5 M in $NaClO_4$ at 25 °C measured against a reference cell containing a solution 8.0×10^{-5} M in $Fe(ClO_4)_3$, 0.20 M in $HClO_4$, and 2.5 M in $NaClO_4$.

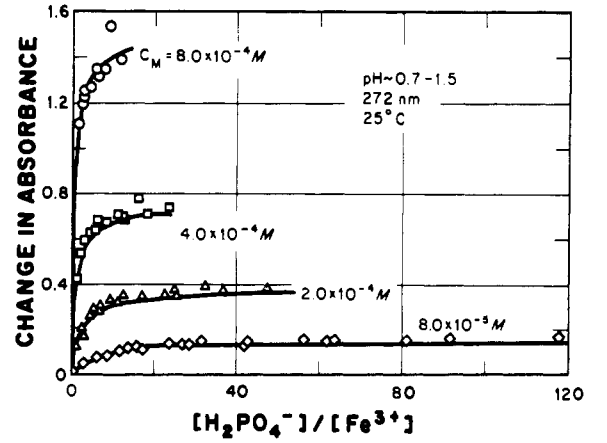

Figure 2. Change in optical absorbance at 272 nm and 25 °C as a function of the initial phosphate ion concentration to ferric ion ratio. The four curves are for different ferric ion concentrations. The pH of the samples varied between 0.7 and 1.5. The solid lines represent the predicted values from a computer modeling program for the species $FeH_2PO_4^{2+}$.

The spectra of dilute ferric salt solutions in the absence of phosphate ions were obtained by using water in the reference cell. In all cases in which the sample contained ferric and phosphate ions, the reference solution was comprised of a similar concentration of ferric perchlorate, perchloric acid, and sodium perchlorate. Since phosphoric acid alone did not absorb light under the experimental conditions studied, the measured absorbance difference (ΔA) was due to the formation of the ferric phosphate complex(es).

Stopped-Flow Measurements. An improved version of a combined stopped-flow temperature-jump apparatus already described in detail elsewhere,[26] was used to obtain thermodynamic and kinetic parameters of the ferric phosphate complexation reactions.

Results

Equilibrium Studies. Absorbance measurements were used to determine the stability constants of complexes of ferric ions with phosphoric acid. A clearly discernible change in absorbance (as determined in a Perkin-Elmer spectrophotometer) due to the presence of the phosphate ion in aqueous solutions containing the ferric ion is shown in Figure 1. The maximum change in absorbance occurred at 278 nm and was a function of iron(III), phosphate, and hydrogen ion concentrations. Even though the experiments were performed at pH <2, the presence of the $FeOH^{2+}$ complex would contribute to the absorption of light at

(9) Filatova, L. N. *Russ. J. Inorg. Chem.* (*Engl. Transl.*) **1974**, *19*, 1827.
(10) Kim, M. S.; Kim, C. H.; Sohn, Y. S. *Taehan Hwahakhoe Chi* **1975**, 19, 325.
(11) Filatova, L. N.; Shelyakina, M. A.; Plachinoda, A. S.; Makarov, E. F. *Russ. J. Inorg. Chem.* (*Engl. Transl.*) **1976**, *21*, 1494.
(12) Salmon, J. E. *J. Chem. Soc.* **1952**, 2316.
(13) Salmon, J. E. *J. Chem. Soc.* **1953**, 2644. Holroyd, A.; Salmon, J. E. *J. Chem. Soc.* **1956**, 269.
(14) Jameson, R. F.; Salmon, J. E. *J. Chem. Soc.* **1954**, 28.
(15) Holroyd, A.; Salmon, J. E. *J. Chem. Soc.* **1957**, 959.
(16) Filatova, L. N.; Shelyakina, M. A. *Russ. J. Phys. Chem.* (*Engl. Transl.*) **1974**, *48*, 1700.
(17) Filatova, L. N.; Galochkina, G. V. *Russ. J. Inorg. Chem.* (*Engl. Transl.*) **1974**, *19*, 1675; **1978**, *23*, 369.
(18) Jensen, K. *Z. Anorg. Allg. Chem.* **1934**, *1*, 221.
(19) Faucherre, J.; Msika, D. *Bull. Soc. Chim. Fr.* **1962**, 1824.
(20) Ciavatta, L. *Ann. Chim.* (*Rome*) **1974**, *64*, 667.
(21) Holroyd, A.; Jameson, R. F.; Odell, A. L.; Salmon, J. E. *J. Chem. Soc.* **1957**, 3239.
(22) Ram, A.; Bose, A. K.; Kumar, S. *J. Sci. Ind. Res.* **1954**, *133*, 217.
(23) Wilhelmy, R. B.; Matijević, E., submitted for publication in *Colloids Surf.*
(24) Moss, M. L.; Mellon, M. G. *Ind. Eng. Chem., Anal. Ed.* **1942**, *14*, 862.
(25) Murphy, J.; Riley, J. P. *Anal. Chim. Acta* **1962**, *27*, 31.
(26) Patel, R. C. *Chem. Instrum.* (*N.Y.*) **1976**, *7*, 83.

this wavelength. An isosbestic point in the Fe^{3+}–$FeOH^{2+}$ spectrum was found at 272 nm in agreement with the literature value;[27] thus, all subsequent equilibrium and kinetic studies were carried out at this wavelength. The extinction coefficient for this wavelength was determined to be 1520 cm^2 mol^{-1} at 25 °C and 1590 cm^2 mol^{-1} at 50 °C.

The reversibility of the reaction was established by cooling several samples from 50 to 25 °C. The absorbances agreed, within experimental error, with those measured at room temperature, also indicating that no solid phase formed on heating such solutions to 50 °C.

In order to tentatively identify the number and the composition of complexes present at equilibrium, the absorbance data (Table II) were analyzed by using a modified version of the mole ratio method described by Yoe and Jones.[28] A reasonable series of curves was obtained with $H_2PO_4^-$ as the ligand and Fe^{3+} as the metal ion species (Figure 2). From the intersection of the tangents it was estimated that a 1:1 complex was formed with an extinction coefficient of approximately 3500 cm^2 mol^{-1}. This method indicated only one complex species in the system.

The data were then analyzed by using curve-fitting procedures to obtain quantitative estimates of the formation constant and extinction coefficient and to detect subtle deviations requiring a more sophisticated model. The expressions necessary to describe the change in absorbance due to the formation of ferric phosphate complexes were greatly simplified by using values obtained at the Fe^{3+}–$FeOH^{2+}$ isosbestic point. At low pH and low ferric ion concentrations, the absorbance of the ferric salt solutions in the absence (A') and in the presence (A) of the phosphate ion can be expressed, respectively, as

$$A' = l\epsilon_{is}([Fe^{3+}]' + [FeOH^{2+}]') = l\epsilon_{is}C_M \quad (1)$$

$$A = l(\epsilon_{is}([Fe^{3+}] + [FeOH^{2+}]) + \sum\epsilon_n[complex_n]) \quad (2)$$

where l is the cell path length, ϵ_{is} is the molar extinction coefficient for iron(III) at the isosbestic point, ϵ_n is the molar extinction coefficient of the nth ferric phosphate complex, and C_M is the total analytical concentration of iron(III). In the presence of phosphate, the mass balance expression is

$$C_M = [Fe^{3+}] + [FeOH^{2+}] + \sum m_n[complex_n] \quad (3)$$

where m_n represents the number of iron atoms in the nth complex. Since the measurements were carried out with identical iron concentrations in both sample and reference solutions, the difference in optical absorbance due to the presence of the phosphate ion can be expressed solely as a function of the ferric phosphate complexes present:

$$\Delta A = A - A' = l\sum(\epsilon_n - m_n\epsilon_{is}[complex_n]) \quad (4)$$

This expression is valid for both equilibrium and nonequilibrium conditions.

For the system at equilibrium

$$Fe^{3+} + H_2PO_4^- \overset{K}{\rightleftharpoons} FeH_2PO_4^{2+}$$

the mass action law gives

$$K = \frac{[FeH_2PO_4^{2+}]}{[Fe^{3+}][H_2PO_4^-]} = \frac{[FeH_2PO_4^{2+}][H^+]}{K_d[Fe^{3+}][H_3PO_4]} \quad (5)$$

where K is the formation constant for the complex and K_d is the first dissociation constant for phosphoric acid. The change in absorbance can then be expressed as

$$\Delta A = l\Delta\epsilon K[Fe^{3+}][H_2PO_4^-] \quad (6)$$

where

$$\Delta\epsilon = \epsilon_{FeH_2PO_4^{2+}} - \epsilon_{is} \quad (7)$$

For systems at equilibrium at low pH, low concentrations of iron(III), and at least a tenfold excess of phosphoric acid over the metal ion concentration, the appropriate mass balance approximations are

$$[H_2PO_4^-] = \{[(C_H + K_d)^2 + 4K_dC_L]^{1/2} - (C_H + K_d)\}/2 \quad (8)$$

$$[H^+] = C_H + [H_2PO_4^-] \quad (9)$$

$$[Fe^{3+}] = C_M/\{1 + (K_h + KK_dC_L)/[H^+]\} \quad (10)$$

where C_H is the perchloric acid concentration, K_h is the hydrolysis constant for iron(III), and C_L is the total analytical concentration of the phosphate. Thus, the change in absorbance is a function of known quantities C_M, C_L, C_H, K_d, and K_h and of two parameters that need to be evaluated, $\Delta\epsilon$ and K. Expressions were derived for various complexes including $Fe(H_xPO_4)^{x+}$ and $Fe(OH)_y(H_xPO_4)^{(x-y)+}$, as well as for dinuclear ferric and/or diphosphate species.

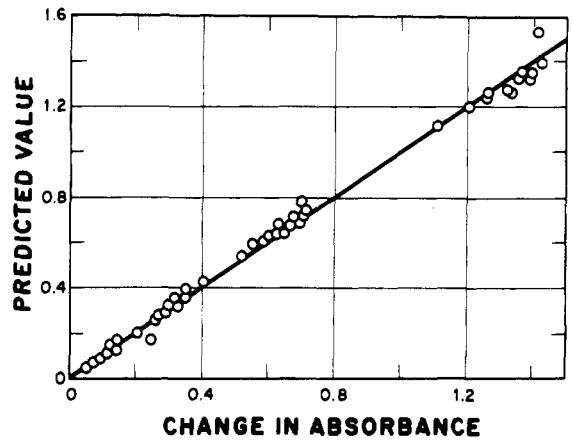

Figure 3. Correlation diagram between the experimental change in absorbance and the value predicted for the formation of $FeH_2PO_4^{2+}$ (ϵ = 3340 cm^2 mol^{-1}, log K = 3.49).

In agreement with the earlier graphical analysis, a reasonable fit was obtained only when the assumed species was $FeH_2PO_4^{2+}$. The solid lines in Figure 2 represent the predicted change in absorbance due to formation of this complex. Within the accuracy of static spectroscopic data it was not reasonable to postulate the existence of another species (Figure 3). There was no indication that a $FeHPO_4^+$ species formed in the solution studied. Table III lists the estimated parameters from the static spectroscopic measurements as well as those estimated from the amplitudes of the stopped-flow experiments. It was observed that the value of the formation constant was somewhat dependent on the estimate of the extinction coefficient. Thus, log K varied between 3.57 ± 0.04 and 3.45 ± 0.04 as ϵ was raised from 3300 to 3410 cm^2 mol^{-1}. The extinction coefficient obtained from the stopped-flow experiments is somewhat higher as a result of the larger slit widths commonly used in the kinetic experiments. Since the equilibrium constant does not change much with temperature, the enthalpy of the reaction must be small. This finding was independently verified by temperature-jump relaxation experiments in which no difference in optical absorbances were detected with a 4.0 °C temperature jump.

Kinetic Studies. Since the experimental conditions had been chosen such that one of the reactants, notably phosphoric acid, was in large excess, the reactions were treated as noncoupled pseudo-first-order processes:

$$A = A_0 + \sum A_i e^{-t/\tau_i} \quad (11)$$

where A is the absorbance at time t, A_0 is the initial absorbance

(27) (a) Sylva, R. N. *Rev. Pure Appl. Chem.* **1972**, *22*, 115. (b) Baes, R. N.; Mesner, R. E. "The Hydrolysis of Cations"; Wiley: New York, 1976.
(28) (a) Yoe, J. H.; Jones, A. L. *Ind. Eng. Chem., Anal. Ed.* **1944**, *16*, 111. (b) Rossotti, F. J. C.; Rossotti, H. "The Determination of Stability Constants"; McGraw-Hill: New York, 1961; p 52. (c) Beck, M. T. "Chemistry of Complex Equilibria"; Van Nostrand Reinhold: London, 1970; p 89.
(29) Martell, A. E.; Sillén, L. G. *Spec. Publ.—Chem. Soc.* **1964**, *No. 17*.
(30) Sapieszko, R. S.; Patel, R. C.; Matijević, E. *J. Phys. Chem.* **1977**, *81*, 1061.

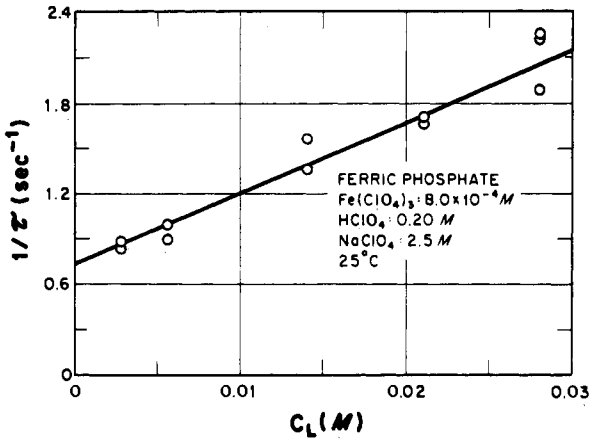

Figure 4. Plot of the reciprocal values of the characteristic time constant τ as a function of C_L for $C_M = 8.0 \times 10^{-4}$ M and $C_H = 0.20$ M. The data fit eq 12 for first-order kinetics.

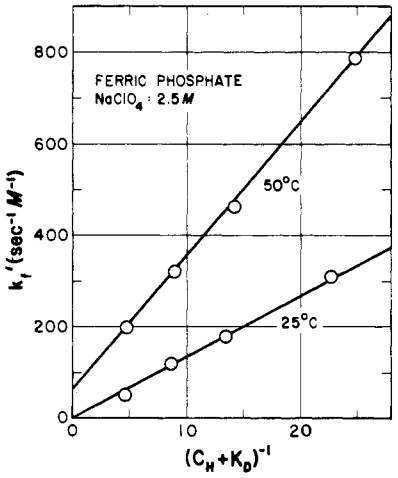

Figure 5. Apparent forward rate constant k_f' for the formation of $FeH_2PO_4^{2+}$ plotted as a function of the inverse value of the hydrogen ion concentration $(C_H + K_D)^{-1}$.

(due to Fe^{3+} and $FeOH^{2+}$), A_i is the total change in absorbance due to the ith reaction, and τ_i is the characteristic time constant for that reaction. The time constant is the inverse of the observed rate constant, k_{obsd}:

$$1/\tau = k_{obsd} = k_f C_L + k_b \qquad (12)$$

Estimates of the values of the forward and backward rate constants were obtained from the slope and the intercept, respectively, of plots of $1/\tau$ vs. C_L (if all other experimental parameters are kept unchanged) (Figure 4). The uncertainty associated with determining the intercept is relatively large, so that the backward rate constant was also determined from the ratio of the forward rate constant to the formation constant. The functional dependence of the observed rate constants on other experimental conditions can then be ascertained.

In the stopped-flow experiments, the increase in optical density due to the first reaction process was attributed to the formation of $FeH_2PO_4^{2+}$. There are three second-order reaction pathways that would account for this product under prevailing experimental conditions:

path 1 $$Fe^{3+} + H_3PO_4 \underset{k_{-1}}{\overset{k_1}{\rightleftharpoons}} FeH_2PO_4^{2+} + H^+ \qquad (13)$$

path 2 $$Fe^{3+} + H_2PO_4^- \underset{k_{-2}}{\overset{k_2}{\rightleftharpoons}} FeH_2PO_4^{2+} \qquad (14)$$

path 3 $$FeOH^{2+} + H_3PO_4 \underset{k_{-3}}{\overset{k_3}{\rightleftharpoons}} FeH_2PO_4^{2+} \qquad (15)$$

Figure 5 demonstrates the inverse hydrogen ion dependency of the forward rate constant under conditions of excess added acid

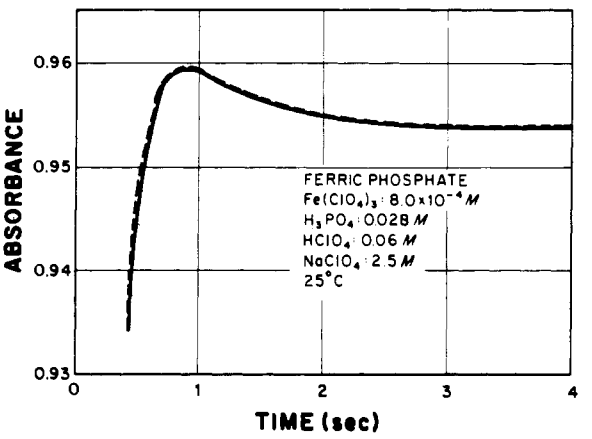

Figure 6. Stopped-flow experiment displaying two chemical processes. The initial conditions upon mixing were 8.0×10^{-4} M in $Fe(ClO_4)_3$, 0.028 M in H_3PO_4, 0.06 M in $HClO_4$, and 2.5 M in $NaClO_4$ at 25 °C. The heavy dashed line is the superimposed computer-fitted model over the experimental data.

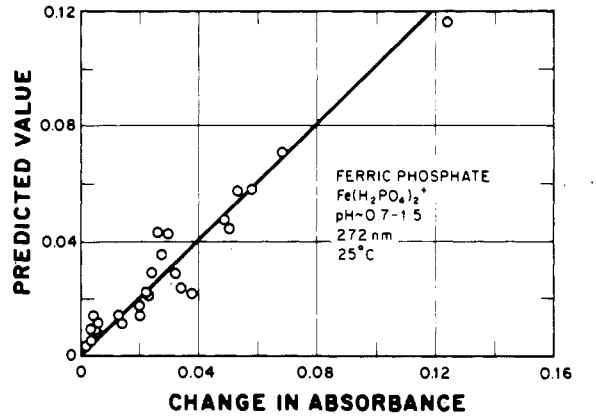

Figure 7. Correlation diagram for the values of the amplitude of the second chemical process in the stopped-flow experiments at 25 °C vs. the predicted values, assuming that $Fe(H_2PO_4)_2^+$ was formed (ϵ = 780 cm^2 mol^{-1}, log K_2 = 4.93).

(Table II) and indicates that a major pathway for the formation of $FeH_2PO_4^{2+}$ is given either by eq 14 or eq 15 or by a combination of the two. For path 2

$$k_2 \simeq k_f(C_H + K_d)/K_d \qquad (16)$$

and for path 3

$$k_3 \simeq k_f(C_H + K_d)/K_h \qquad (17)$$

In view of the positive intercept, path 1 may occur to some extent at elevated temperatures. Since there was no observed dependency of the apparent backward rate constant on the hydrogen ion concentration, the latter appears to be insignificant. Due to the fact that such protonation reactions occur on the time scale of 10^{-9} s, it is not possible to unambiguously determine whether pathway 2, 3, or a combination of the two, predominates. However, a distinction can be arrived at by the evaluation of the rate constants and corresponding activation parameters $\Delta H^\ddagger$ and $\Delta S^\ddagger$ (Table IV).

Under some experimental conditions, notably at high phosphate and low perchloric acid concentrations, a second effect could be observed; i.e., the absorbance initially increased and then decreased (Figure 6). The amplitudes of the second effect, obtained by a computer modeling procedure, were found to correlate with the formation of $Fe(H_2PO_4)_2^+$. The correlation between the observed and predicted changes in absorbance due to the species $Fe(H_2PO_4)_2^+$ is shown in Figure 7. The estimated physical constants are listed in Table V, where

$$K_2 = \frac{[Fe(H_2PO_4)_2^+]}{[Fe^{3+}][H_2PO_4^-]^2} \qquad (18)$$

Table II. Iron Phosphate Solution Chemistry Data

init concn, M			T = 25 °C						T = 50 °C					
$[HClO_4]$ (CH)	$[Fe(ClO_4)_3]$ (CM)	$[H_3PO_4]$ (CL)	A_{272}[a]	ΔA_{272}[a]	A_{272}[b]	τ_1,[b] s	ΔA_1[b]	τ_2,[b] s	ΔA_2[b]	A_{272}[a]	ΔA_{272}[a]	A_{272}[b]	τ_1,[b] s	ΔA_1[b]	τ_2,[b] s	ΔA_2[b]
3.0×10^{-2}	8.0×10^{-5}	0.0	0.126		0.035					0.135		0.033				
		2.8×10^{-3}		0.115		4.1×10^{-1}	2.9×10^{-2}				0.113		1.2×10^{-1}	2.9×10^{-2}		
		5.6×10^{-3}		0.132		3.8×10^{-1}	3.3×10^{-2}	4.2	1.5×10^{-3}		0.126		8.3×10^{-2}	3.5×10^{-2}	6.0×10^{-4}	5.4×10^{-3}
		1.4×10^{-2}		0.152		1.9×10^{-1}	4.1×10^{-2}	1.7	5.0×10^{-3}		0.148		5.3×10^{-2}	4.0×10^{-2}	3.4×10^{-1}	1.1×10^{-2}
		2.1×10^{-2}		0.162		1.3×10^{-1}	4.3×10^{-2}	1.0	5.9×10^{-3}		0.159		4.4×10^{-2}	4.3×10^{-2}	3.5×10^{-1}	5.3×10^{-3}
		2.8×10^{-2}		0.169		1.0×10^{-1}	4.7×10^{-2}	8.9×10^{-1}	4.2×10^{-3}		0.168		3.4×10^{-2}	4.5×10^{-2}		
	2.0×10^{-4}	0.0	0.313		0.101					0.332		0.102				
		2.8×10^{-3}		0.292		4.8×10^{-1}	7.9×10^{-2}				0.277		1.5×10^{-1}	6.9×10^{-2}		
		5.6×10^{-3}		0.317		3.2×10^{-1}	8.7×10^{-2}	2.5	3.6×10^{-3}		0.303		1.1×10^{-1}	8.2×10^{-2}		
		1.4×10^{-2}		0.352		1.7×10^{-1}	9.9×10^{-2}	8.8×10^{-1}	2.3×10^{-2}		0.333		6.5×10^{-2}	9.5×10^{-2}	3.9×10^{-1}	2.0×10^{-2}
		2.1×10^{-2}		0.369		1.3×10^{-1}	1.1×10^{-1}	6.7×10^{-1}	2.4×10^{-2}		0.353		4.8×10^{-2}	1.0×10^{-1}	2.5×10^{-1}	2.4×10^{-2}
		2.8×10^{-2}		0.387		1.0×10^{-1}	1.1×10^{-1}	4.7×10^{-1}	2.7×10^{-2}		0.373		4.6×10^{-2}	1.1×10^{-1}	2.0×10^{-1}	3.2×10^{-2}
	4.0×10^{-4}	0.0	0.622		0.199					0.642		0.196				
		5.6×10^{-3}		0.637		3.3×10^{-1}	1.9×10^{-1}				0.596		1.1×10^{-1}	2.1×10^{-1}		
		1.4×10^{-2}		0.686		1.6×10^{-1}	2.2×10^{-1}	9.1×10^{-1}	2.9×10^{-2}		0.647		5.0×10^{-2}	2.3×10^{-1}		
		2.1×10^{-2}		0.710		1.2×10^{-1}	2.3×10^{-1}	4.7×10^{-1}	5.8×10^{-2}		0.670		3.8×10^{-2}	2.5×10^{-1}		
		2.8×10^{-2}		0.739		1.1×10^{-1}	2.5×10^{-1}	3.4×10^{-1}	6.8×10^{-2}		0.700		3.5×10^{-2}	2.6×10^{-1}		
	8.0×10^{-4}	0.0	1.188		0.430					1.266		0.426				
		1.4×10^{-2}		1.320		1.5×10^{-1}	5.0×10^{-1}	5.1×10^{-1}	2.9×10^{-2}		1.246		4.5×10^{-2}	5.5×10^{-1}		
		2.1×10^{-2}		1.531		1.2×10^{-1}	5.4×10^{-1}	2.5×10^{-1}	1.2×10^{-1}		1.297		3.6×10^{-2}	6.0×10^{-1}		
		2.8×10^{-2}		1.388		9.3×10^{-2}	5.3×10^{-1}	2.4×10^{-1}	6.1×10^{-2}		1.317		3.5×10^{-2}	6.4×10^{-1}		
6.0×10^{-2}	8.0×10^{-5}	0.0	0.110		0.037					0.133		0.033				
		2.8×10^{-3}		0.085		1.5	1.5×10^{-2}				0.086		1.9×10^{-1}	1.9×10^{-2}		
		5.6×10^{-3}		0.108		1.0	2.0×10^{-2}				0.110		1.6×10^{-1}	2.5×10^{-2}		
		1.4×10^{-2}		0.131		4.1×10^{-1}	2.7×10^{-2}	2.1	3.5×10^{-3}		0.133		1.0×10^{-1}	3.1×10^{-2}	8.7×10^{-1}	4.2×10^{-3}
		2.1×10^{-2}		0.148		2.8×10^{-1}	3.3×10^{-2}	1.5	4.8×10^{-3}		0.140		7.4×10^{-2}	2.8×10^{-2}	2.3×10^{-1}	2.8×10^{-2}
		2.8×10^{-2}		0.152		2.7×10^{-1}	3.2×10^{-2}	1.2	4.8×10^{-3}		0.151		7.0×10^{-2}	3.0×10^{-2}	3.0×10^{-1}	9.0×10^{-3}
	2.0×10^{-4}	0.0	0.290		0.098					0.330		0.090				
		2.8×10^{-3}		0.170		1.6	4.0×10^{-2}				0.227		1.8×10^{-1}	6.6×10^{-2}		
		5.6×10^{-3}		0.302		1.0	6.2×10^{-2}				0.269		1.6×10^{-1}	8.2×10^{-2}		
		1.4×10^{-2}		0.344		4.6×10^{-1}	7.1×10^{-2}	1.8	1.4×10^{-2}		0.308		9.1×10^{-2}	1.0×10^{-1}	6.9×10^{-1}	1.1×10^{-2}
		2.1×10^{-2}		0.372		2.8×10^{-1}	7.8×10^{-2}	1.1	2.0×10^{-2}		0.322		8.0×10^{-2}	1.1×10^{-1}	7.9×10^{-1}	1.2×10^{-2}
		2.8×10^{-2}		0.391		2.3×10^{-1}	8.4×10^{-2}	8.0×10^{-1}	2.2×10^{-2}		0.346		6.0×10^{-2}	1.1×10^{-1}	1.9×10^{-1}	4.4×10^{-2}
	4.0×10^{-4}	0.0	0.603		0.218					0.642		0.190				
		5.6×10^{-3}		0.603		9.1×10^{-1}	1.5×10^{-1}				0.540		1.3×10^{-1}	1.8×10^{-1}		
		1.4×10^{-2}		0.662		3.7×10^{-1}	1.7×10^{-1}	1.3	3.4×10^{-2}		0.603		7.5×10^{-2}	2.1×10^{-1}	3.3×10^{-1}	3.2×10^{-2}
		2.1×10^{-2}		0.701		2.5×10^{-1}	1.9×10^{-1}	9.7×10^{-1}	4.6×10^{-2}		0.628		7.5×10^{-2}	2.3×10^{-1}	2.1×10^{-1}	7.5×10^{-2}
		2.8×10^{-2}		0.779		2.1×10^{-1}	2.1×10^{-1}	6.4×10^{-1}	5.0×10^{-2}		0.659		5.2×10^{-2}	2.5×10^{-1}	1.4×10^{-1}	1.3×10^{-1}
	8.0×10^{-4}	0.0	1.206		0.429					1.266		0.441				
		1.4×10^{-2}		1.260		2.5×10^{-1}	4.7×10^{-1}	9.0×10^{-1}	4.9×10^{-2}		1.153		8.0×10^{-2}	4.7×10^{-1}	2.7×10^{-1}	4.2×10^{-2}
		2.1×10^{-2}		1.345		1.7×10^{-1}	4.9×10^{-1}	1.1	2.0×10^{-2}		1.190		6.8×10^{-2}	5.0×10^{-1}	2.2×10^{-1}	9.3×10^{-2}
		2.8×10^{-2}		1.347		1.4×10^{-1}	5.3×10^{-1}	5.4×10^{-1}	3.9×10^{-2}		1.233		5.1×10^{-2}	6.2×10^{-1}	1.8×10^{-1}	1.5×10^{-1}
1.0×10^{-1}	8.0×10^{-5}	0.0	0.128		0.039					0.136		0.035				
		2.8×10^{-3}		0.073		1.4	1.6×10^{-2}				0.070		3.1×10^{-1}	1.6×10^{-2}		
		5.6×10^{-3}		0.101		1.1	2.4×10^{-2}				0.097		2.3×10^{-1}	2.4×10^{-2}		
		1.4×10^{-2}		0.134		7.0×10^{-4}	3.3×10^{-2}	6.8	1.4×10^{-3}		0.126		1.3×10^{-1}	3.3×10^{-2}	1.2	1.9×10^{-3}
		2.1×10^{-2}		0.145		4.0×10^{-1}	3.7×10^{-2}	2.4	2.7×10^{-3}		0.140		1.1×10^{-1}	3.8×10^{-2}	5.7×10^{-1}	9.0×10^{-3}
		2.8×10^{-2}		0.159		2.9×10^{-1}	4.1×10^{-2}	1.6	3.3×10^{-3}		0.145		8.0×10^{-2}	4.0×10^{-2}	5.1×10^{-1}	4.1×10^{-3}
	2.0×10^{-4}	0.0	0.311		0.101					0.333		0.089				
		2.8×10^{-3}		0.193		1.1	5.3×10^{-2}				0.187		4.8×10^{-1}	4.9×10^{-2}		
		5.6×10^{-3}		0.260		1.1	5.4×10^{-2}				0.241		3.4×10^{-1}	6.9×10^{-2}		
		1.4×10^{-2}		0.321		6.5×10^{-1}	7.2×10^{-2}				0.302		1.5×10^{-1}	9.3×10^{-2}		

		2.1×10^{-2}		0.347		4.0×10^{-1}	9.0×10^{-2}	1.5	1.4×10^{-2}		0.323		1.2×10^{-1}	1.0×10^{-1}		
		2.8×10^{-2}		0.363		2.9×10^{-1}	1.0×10^{-1}	1.4	1.2×10^{-2}		0.339		1.0×10^{-1}	1.1×10^{-1}		
	4.0×10^{-4}	0.0	0.624		0.202					0.656		0.191				
		5.6×10^{-3}		0.539		1.1	1.3×10^{-1}				0.505		3.1×10^{-1}	1.6×10^{-1}		
		1.4×10^{-2}		0.638		4.5×10^{-1}	1.7×10^{-1}	1.6	2.0×10^{-2}		0.592		1.7×10^{-1}	2.0×10^{-1}	4.3×10^{-1}	1.5×10^{-2}
		2.1×10^{-2}		0.672		3.2×10^{-1}	2.0×10^{-1}	1.2	3.7×10^{-2}		0.621		1.3×10^{-1}	2.1×10^{-1}	4.7×10^{-1}	4.2×10^{-2}
		2.8×10^{-2}		0.707		2.7×10^{-1}	2.2×10^{-1}	1.0	3.2×10^{-2}		0.650		1.1×10^{-1}	2.2×10^{-1}	3.5×10^{-1}	4.2×10^{-2}
	8.0×10^{-4}	0.0	1.215		0.454					1.278		0.420				
		1.4×10^{-2}		1.233		4.1×10^{-1}	4.3×10^{-1}				1.137		1.6×10^{-1}	7.6×10^{-1}		
		2.1×10^{-2}		1.270		3.3×10^{-1}	3.1×10^{-1}	1.0	2.6×10^{-2}		1.179		1.1×10^{-1}	6.2×10^{-1}	6.4×10^{-1}	6.2×10^{-2}
		2.8×10^{-2}		1.321		2.3×10^{-1}	3.6×10^{-1}	1.3	5.3×10^{-2}		1.215		8.6×10^{-1}	6.4×10^{-1}	3.2×10^{-1}	7.0×10^{-2}
2.0×10^{-1}	8.0×10^{-5}	0.0	0.117		0.035					0.134		0.032				
		2.8×10^{-3}		0.050		1.2	1.7×10^{-2}				0.044		9.1×10^{-1}	6.6×10^{-3}		
		5.6×10^{-3}		0.077		1.1	2.4×10^{-2}				0.069		5.8×10^{-1}	1.6×10^{-2}		
		1.4×10^{-2}		0.121		6.8×10^{-1}	3.6×10^{-2}				0.108		2.4×10^{-1}	2.9×10^{-2}		
		2.1×10^{-2}		0.137		5.9×10^{-1}	3.6×10^{-2}				0.120		2.0×10^{-1}	3.3×10^{-2}		
		2.8×10^{-2}		0.149		4.5×10^{-1}	4.2×10^{-2}				0.131		1.6×10^{-1}	3.6×10^{-2}		
	2.0×10^{-4}	0.0	0.306		0.075					0.326	0.087					
		2.8×10^{-3}		0.123		1.1	5.0×10^{-2}				0.117		6.5×10^{-1}	2.9×10^{-2}		
		5.6×10^{-3}		0.200		9.8×10^{-1}	7.4×10^{-2}				0.183		4.6×10^{-1}	5.1×10^{-2}		
		1.4×10^{-2}		0.286		7.2×10^{-1}	9.6×10^{-2}				0.270		2.7×10^{-1}	7.7×10^{-2}		
		2.1×10^{-2}		0.328		5.6×10^{-1}	1.0×10^{-1}				0.298		2.2×10^{-1}	8.8×10^{-2}		
		2.8×10^{-2}		0.348		4.4×10^{-1}	1.1×10^{-1}				0.317		1.4×10^{-1}	9.2×10^{-2}		
	4.0×10^{-4}	0.0	0.617		0.196					0.650		0.191				
		5.6×10^{-3}		0.425		1.6	1.4×10^{-1}				0.386		4.8×10^{-1}	1.3×10^{-1}		
		1.4×10^{-2}		0.592		1.0	2.0×10^{-1}				0.539		3.1×10^{-1}	1.9×10^{-1}		
		2.1×10^{-2}		0.632		7.4×10^{-1}	2.1×10^{-1}				0.587		2.3×10^{-1}	2.0×10^{-1}		
		2.8×10^{-2}		0.678		5.9×10^{-1}	2.3×10^{-1}				0.619		1.6×10^{-1}	2.1×10^{-1}		
	8.0×10^{-4}	0.0	1.245		0.451					1.260		0.409				
		1.4×10^{-2}		1.111		1.0	4.3×10^{-1}				1.054		2.6×10^{-1}	4.0×10^{-1}		
		2.1×10^{-2}		1.194		6.6×10^{-1}	4.3×10^{-1}				1.114		1.8×10^{-1}	4.2×10^{-1}		
		2.8×10^{-2}		1.252		4.8×10^{-1}	4.6×10^{-1}				1.174		1.6×10^{-1}	4.0×10^{-1}		

[a] UV/visible spectrophotometric measurements: cell path length 1.0 cm. [b] Stopped-flow spectrophotometric measurements: apparent cell path length 0.33 cm.

Table III. Formation Constants (μ = 2.5 M $NaClO_4$) and Extinction Coefficients (λ = 272 nm) for $FeH_2PO_4^{2+}$ [a]

	25 °C		50 °C		
	log K	ϵ, cm^2 mol^{-1}	log K	ϵ, cm^2 mol^{-1}	ref
spectrophotometry	3.49 ± 0.07	3340 ± 60	3.69 ± 0.06	3250 ± 60	this work
stopped flow	3.47 ± 0.09	3340 ± 60	3.28 ± 0.14	4030 ± 60	this work
lit. data	3.60 ± 0.10 (μ = 0.1 M)				8
	3.46 ± 0.05 (μ = 0.4 M)				5
	3.18 ± 0.05 (μ = 3.0 M)				20

[a] Values for K_d used in the calculations were 0.014 (25 °C) and 0.0103 (50 °C)[29] and for K_h were 1.19×10^{-3} (25 °C) and 3.43×10^{-3} (50 °C).[30]

Table IV. Summary of Kinetic Information for the Formation of $FeH_2PO_4^{2+}$

pathway	$k_{25°C}$, s^{-1}	$k_{50°C}$, s^{-1}	ΔH^*, kcal mol^{-1}	ΔS^*, cal deg^{-1} mol^{-1}
1	~0	60		
combined 2 + 3	13.4 (k_2K_d + k_3K_h)	29.2		
if pathway 2 predominates	6.8×10^4	2.7×10^5	9.9	−3.0
if pathway 3 predominates	9.2×10^6	2.4×10^6	−10.8	−63
k_b	0.61	3.3	12	−18

Table V. Physical Constants for $Fe(H_2PO_4)_2^+$

T, °C	ϵ, cm^2 mol^{-1}	log K_2
25	780 ± 150	4.9 ± 0.6
50	930 ± 250	5.2 ± 1.4

There is little effect of temperature on the value of K_2. The spectroscopic study evidently was not able to distinguish the small contribution to the total absorbance made by the diphosphate complex. Only the time-resolved kinetic study allowed identification of the complex.

In the analysis of the kinetic data, the following reaction pathways were considered:

$$\text{path 4}\quad FeH_2PO_4^{2+} + H_3PO_4 \underset{k_{-4}}{\overset{k_4}{\rightleftharpoons}} Fe(H_2PO_4)_2^+ + H^+ \qquad (19)$$

$$\text{path 5}\quad FeH_2PO_4^{2+} + H_2PO_4^- \underset{k_{-5}}{\overset{k_5}{\rightleftharpoons}} Fe(H_2PO_4)_2^+ \qquad (20)$$

$$\text{path 6}\quad FeH_2PO_4^{2+} \rightleftharpoons Fe(OH)(H_2PO_4)^+ + H^+ \qquad (21)$$

The equilibrium constant for the rapid step (eq 21) is characterized by K_h', and is followed by the slower complexation reaction:

$$Fe(OH)(H_2PO_4)^+ + H_2PO_4^- \underset{k_{-6}}{\overset{k_6}{\rightleftharpoons}} Fe(OH)(H_2PO_4)_2 \qquad (22)$$

$$Fe(OH)(H_2PO_4)_2 + H^+ \rightleftharpoons Fe(H_2PO_4)_2^+ \quad \text{rapid} \qquad (23)$$

$$\text{path 7}\quad Fe(OH)(H_2PO_4)^+ + H_3PO_4 \underset{k_{-7}}{\overset{k_7}{\rightleftharpoons}} Fe(H_2PO_4)_2^+ \qquad (24)$$

Since the total phosphate concentration was in large excess, data were treated according to the pseudo-first-order kinetics. A calculation of the species distribution revealed that the concentration of free Fe^{3+} was much smaller than that of $FeH_2PO_4^{2+}$ and $Fe(H_2PO_4)_2^+$. Analogous to the previous analysis (eq 12), the respective forward and backward rate constants are given by

$$k_f' = (k_4[H^+] + k_5K_d + (k_6K_dK_h')/[H^+] + k_7K_h')/([H^+] + K_d) \qquad (25)$$

$$k_b' = k_{-4}[H^+] + k_{-5} + k_{-6} + k_{-7} \qquad (26)$$

It is convenient to rearrange eq 25 as follows:

$$F([H^+]) = [H^+]([H^+] + K_d)k_f' = k_4[H^+]^2 + [H^+](k_7K_h' + k_5K_d) + k_6k_dK_h' \qquad (27)$$

There was a larger error associated with the determination of these rate constants since there were fewer data points as a result of experimental constraints, which limited the concentration range that could be investigated. A plot of $F([H^+])$ vs. $[H^+]$ is found to be linear with zero intercept at both temperatures (Figure 8), indicating that the values of k_4 and $k_6K_dK_h'$ are negligible. The backward rate constant showed no dependence on pH, and considering the unimportance of the $k_6K_dK_h'$ term, it appears reasonable to equate k_b' to $k_{-5} + k_{-7}$. The relevant kinetic information is listed in Table VI. Without more detailed knowledge of

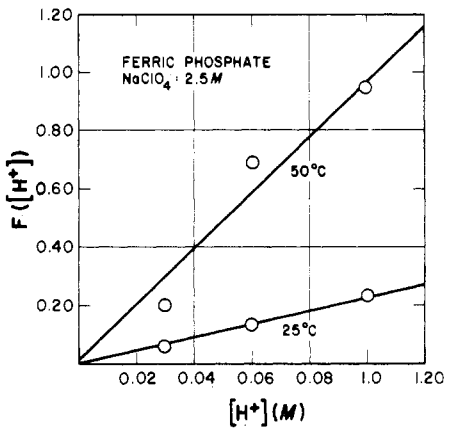

Figure 8. $F([H^+])$ for the formation of $Fe(H_2PO_4)_2^+$ plotted as a function of the hydrogen ion concentration according to eq 27.

Table VI. Summary of Kinetic Data for the Formation of $Fe(H_2PO_4)_2^+$

$(k_5K_d + k_7K_h')$ at 25 °C	2.3 s^{-1}
$(k_5K_d + k_7K_h')$ at 50 °C	9.7 s^{-1}
k_5(maximum) at 25 °C	160 M^{-1} s^{-1}
ΔH_{obsd}^*(forward)	10.5 kcal mol^{-1}
ΔH_{obsd}^*(backward)	12 kcal mol^{-1}
ΔS_{obsd}^*(forward)	−22 cal deg^{-1} mol^{-1}
ΔS_{obsd}^*(backward)	−25 cal deg^{-1} mol^{-1}

pathways 6 and 7, analysis of the activation parameters of the individual steps is not feasible. It can be shown that the observed activation enthalpies are given by

$$\Delta H_{obsd}^*(\text{forward}) = [k_7K_h'(\Delta H_h^{\circ\prime} + \Delta H_7^*) + k_5K_d(\Delta H_d^\circ + \Delta H_5^*)]/(k_7K_h' + k_5K_d) \qquad (28)$$

$$\Delta H_{obsd}^*(\text{backward}) = (k_{-5}\Delta H_{-5}^* + k_{-7}\Delta H_{-7}^*)/(k_{-5} + k_{-7}) \qquad (29)$$

Limiting cases pertaining to individual steps can be obtained from eq 27–29. If $k_7 << k_5$, k_5(maximum) $\simeq$ 160 M^{-1} s^{-1} at 25 °C, $\Delta H_5^* \simeq$ 13 kcal mol^{-1}, and $\Delta H_{-5}^* \simeq$ 12 kcal mol^{-1}.

Discussion

The combined equilibrium and kinetic study has shown that two ferric phosphate species formed under experimental conditions similar to those that lead to the formation of uniform ferric phosphate sols. Both the equilibrium and kinetic data are consistent with the formation of $FeH_2PO_4^{2+}$, and the formation constant for the species at 25 °C is in very good agreement with the values reported by other investigators (Table III). Neither the change in enthalpy nor formation constants at elevated temperatures were previously reported. The presence of the monohydrogen species $FeHPO_4^+$ was not detected, though according to the formation constant reported by Galal-Gorchev and Stumm[5] over 30% of the iron should have been incorporated as this species under some of the conditions. If such a large percentage formed, the deviation would be clearly distinguishable in Figures 2 and 3. Also the computer curve-fitting procedure did not provide reasonable fits for either the formation of $FeHPO_4^+$ or a mixture of $FeH_2PO_4^{2+}$ and $FeHPO_4^+$.

The analysis of the kinetic data indicated that, under the conditions studied, the reaction proceeded primarily through a hydrogen ion dependent pathway, though there was a contribution to the overall process that is independent of the H^+ concentration. Further elucidation of the mechanism of $FeH_2PO_4^{2+}$ formation was carried out by assuming that one of the two H^+-dependent pathways predominate. Reactions involving Fe^{3+} have been proposed to follow an associative substitution mechanism in which the nature of the ligand greatly influences the observed rate constant. The value for k_2 (at 25 °C) seems reasonable in light of the previously published results for other ligands.[31] Assuming

$FeOH^{2+}$ as a reactant results in a dissociative ion-pair mechanism, in which the observed forward rate constant should be approximately 2×10^3 M^{-1} s^{-1} for a ligand with zero charge (H_3PO_4) at room temperature. From Table IV the constant k_3 (at 25 °C) of $\sim 9 \times 10^6$ M^{-1} s^{-1} is over 3 orders of magnitude higher. Furthermore, while the activation parameters for ligand substitution should be lower than the values for water solvent exchange, ΔH^* for the reaction involving $FeOH^{2+}$ appears to be much too low when compared to the activation parameters[33] (ΔH^*, ΔS^*) for water exchange (15.3 kcal mol^{-1} and 2.9 cal mol^{-1} deg^{-1} for Fe^{3+}, and 10.14 kcal mol^{-1} and 1.26 cal mol^{-1} deg^{-1} for $FeOH^{2+}$). On this basis, it is proposed that the associative mechanism involving Fe^{3+} is more reasonable. Finally the mechanism of complex formation currently proposed for a number of tervalent cations, including other iron(III)-ligand substitution reactions, is based on associative interchange.[34]

The detection of the ferric diphosphate complex, $Fe(H_2PO_4)_2^+$, demonstrated the value of using a kinetic technique for the characterization of the solution species. While various complex solute species have been postulated (Table I), $Fe(H_2PO_4)_2^+$ was never specifically identified. Under the experimental conditions that lead to the precipitation of uniform dispersions of ferric phosphate particles, significant concentrations of this complex would be present in solution.

Only a few data are found in the literature describing the kinetics of an FeL_2 complex. The observed rate constant for the ferric dichloride species was given as 324 M^{-1} s^{-1}, which is approximately 15 times larger than the rate constant for the formation of the monochloro species,[35] and may be compared with the maximum value of 160 M^{-1} s^{-1} for $Fe(H_2PO_4)_2^+$. In this study, the rate constants for the mono- and diphosphate species showed a wider difference, the ratio being approximately 1:0.002 if a comparison between pathway 2 (Table IV) and k(maximum) (Table VI) is made. Clearly, the type of ligand already present in the inner coordination sphere of iron(III) has a strong influence on the rate of substitution of an additional water molecule. Out of the four parallel pathways that were considered, only two were found to contribute significantly. The activation parameters for both the mono- and diphosphate iron(III) species are listed in Tables IV and VI, and the values appear to be reasonable. As a consequence of the several rapidly established proton-transfer reactions that have to be taken into account, the relative importance of individual steps cannot be clearly assessed, in contrast to the situation with simple ligands such as Cl^-.[35] The formation of $Fe(H_2PO_4)_2^+$ by involving $H_2PO_4^-$ as a reactant also tends to support the formation of the monophosphate species through an analogous pathway.

This work offers strong evidence that the static spectrophotometric procedure may not be sufficiently sensitive to detect successive complexation. In contrast, time-resolved absorbance measurements (e.g. Figure 6) provide an effective method for identification of a series of species in solution.

In conclusion, it appears that the formation of ferric phosphate complexes under these conditions can best be represented by associative mechanisms for both pH-dependent and -independent pathways, in which the hexaaquoiron(III) ion is involved. The recent study by Grant and Jordan[33] supports the view that substitution involving Fe^{3+} is associative interchange while reactions with $FeOH^{2+}$ are dissociative in nature.

Registry No. Fe, 7439-89-6; H_3PO_4, 7664-38-2.

(31) (a) Eigen, M.; Wilkins, R. G. "Mechanisms of Inorganic Reactions"; American Chemical Society: Washington, DC, 1965, Adv. Chem. Ser. No. 49. (b) Wilkins, R. G. "The Study of Kinetics and Mechanism of Reactions of Transition Metal Complexes"; Allyn and Bacon: Boston, 1974. (c) Mentasti, E. *Inorg. Chem.* **1979**, *18*, 1512. (d) Bridger, K.; Patel, R. C.; Matijević, E. *Polyhedron* **1982**, *1*, 269. (e) Ishihara, K.; Funshashi, S.; Tanaka, M. *Inorg. Chem.* **1983**, *22*, 194.
(32) Bjerrum, N.; Dahm, C. R. *Z. Phys. Chem.* **1931**, 627.
(33) Grant, M.; Jordan, R. B. *Inorg. Chem.* **1981**, *20*, 55.
(34) Mentasti, E.; Secco, F.; Venturini, M. *Inorg. Chem.* **1982**, *21*, 2314.
(35) Strahm, E.; Patel, R. C.; Matijević, E. *J. Phys. Chem.* **1979**, *83*, 1689.

Contribution from the Department of Chemistry and the Molecular Structure Center, Indiana University, Bloomington, Indiana 47405

Vanadium(IV) Thiolate Chemistry: Preparation, Structure, and Properties of $[VE(SCH_2CH_2S)_2]^{2-}$ (E = O, S)

JOANNA K. MONEY, JOHN C. HUFFMAN, and GEORGE CHRISTOU*

Received January 25, 1985

The synthesis, structure, and properties of vanadium(IV) complexes with the ethane-1,2-dithiolate ligand (edt^{2-}) are described. $(NMe_4)Na[VO(edt)_2]\cdot 2EtOH$ crystallizes in monoclinic space group $P2_1/n$ with unit cell parameters (at ca. −159 °C) a = 21.312 (5) Å, b = 10.906 (2) Å, c = 9.381 (1) Å, β = 92.77 (1)°, and Z = 4. The vanadium is in a square-pyramidal coordination geometry with the multiply bonded oxygen at the apex (V–O = 1.625 (2) Å) and four ligand sulfur atoms in the base. The anion, cations, and solvent molecules pack into discrete units of C_{2h} symmetry. $[VO(edt)_2]^{2-}$ was cleanly converted into $[VS(edt)_2]^{2-}$ with hexamethyldisilthiane, $(Me_3Si)_2S$. $(PPh_4)Na[VS(edt)_2]\cdot xEt_2O$ crystallizes in triclinic space group $P\bar{1}$ with unit cell parameters (at ca. −160 °C) a = 17.201 (5) Å, b = 10.983 (3) Å, c = 9.919 (3) Å, α = 65.84 (1)°, β = 106.63 (1)°, γ = 93.32 (2)°, and Z = 2. The anion is isostructural with $[VO(edt)_2]^{2-}$ except for the presence of the apical sulfur (V–S = 2.087 (1) Å). The anion, cations, and solvent molecules again pack into discrete dimers, but of a different structure of D_{2h} symmetry. This is only the second example of a structurally characterized species containing the $V{=}S^{2+}$ moiety. Infrared, electrochemical, and UV/visible studies of the two complexes are described.

Introduction

Innumerable complexes of vanadium(IV) containing the vanadyl ($V{=}O^{2+}$) unit have been prepared and studied in detail over the years. In the solid state, such species are predominantly either square pyramidal (VOL_4; L = ligand), with the multiply bonded oxygen atom in the apical position,[1-4] or distorted octahedral (VOL_4L'), in which a sixth ligand (L') has occupied the vacant sixth position trans to the V=O group.[5-8] Other structural variants are also known, but much less common, including trigonal-bipyramidal complexes[9] and one-dimensional polymers due

(1) Selbin, J. *Chem. Rev.* **1965**, *65*, 153; *Coord. Chem. Rev.* **1966**, *1*, 293.
(2) Bruins, D.; Weaver, D. L. *Inorg. Chem.* **1970**, *9*, 130.
(3) Henrick, K.; Raston, C. L.; White, A. H. *J. Chem. Soc., Dalton Trans.* **1976**, 26.
(4) Tapscott, R. E.; Belford, R. L.; Paul, I. C. *Inorg. Chem.* **1968**, *7*, 356.
(5) Form, G. E.; Raper, E. S.; Oughtred, R. E.; Shearer, H. M. M. *J. Chem. Soc., Chem. Commun.* **1972**, 945.
(6) Cotton, F. A.; Lewis, G. E.; Mott, G. N. *Inorg. Chem.* **1982**, *21*, 3127.
(7) Wieghardt, K.; Bossek, U.; Volckmar, K.; Swiridoff, W.; Weiss, J. *Inorg. Chem.* **1984**, *23*, 1387.
(8) Demsar, A.; Bukovec, P. *J. Fluorine Chem.* **1984**, *24*, 369.

0020-1669/85/1324-3297$01.50/0